Amplitude sensing below the zero-point fluctuations with a two-dimensional trapped-ion mechanical oscillator

K. A. Gilmore,[1,2,*] J. G. Bohnet,[1] B. C. Sawyer,[3] J. W. Britton,[4] and J. J. Bollinger[1,†]

[1] *National Institute of Standards and Technology, Boulder, Colorado 80305, USA*
[2] *JILA and Department of Physics, University of Colorado, Boulder, Colorado, 80309, USA*
[3] *Georgia Tech Research Institute, Atlanta, Georgia 30332, USA*
[4] *U.S. Army Research Laboratory, Adelphi, Maryland 20783, USA*

(Dated: March 3, 2017)

We present measurements of the amplitude of a center-of-mass (COM) motion of a two-dimensional ion crystal composed of ∼100 ions in a Penning trap. For motion off-resonant with the trap axial frequency we demonstrate measurements of amplitudes as small as 50 pm, 40 times smaller than the COM mode zero-point fluctuations. The basic technique employs a spin-dependent, optical-dipole force to couple the mechanical oscillation to the electron spins of the trapped ions, enabling a strong measurement of one quadrature of the COM motion through a readout of the spins. We show the limiting sensitivity of the measurement is set by spin projection noise and spin decoherence due to off-resonant light scattering from the optical-dipole force. Variations of the protocol demonstrated here can achieve a sensitivity below 20 pm/$\sqrt{\mathrm{Hz}}$, which will be useful for detecting extremely weak forces (< 1 yN) and electric fields, as well as exploring protocols for probing quantum limits of force detection.

Measuring the amplitude of mechanical oscillators has engaged physicists for more than 50 years [1, 2] and, as the limits of amplitude sensing have dramatically improved, produced exciting advances both in fundamental physics and in applied work. Examples include the detection of gravitational waves [3], the coherent quantum control of mesoscopic objects [4], improved force microscopy [5], and the transduction of quantum signals [6]. During the past decade, optical-mechanical systems have facilitated increasingly sensitive techniques for reading out the amplitude of a mechanical oscillator [7–11], with a recent demonstration obtaining a measurement imprecession more than two orders of magnitude below the size of the ground state wave function (i.e. the amplitude z_{ZPT} of the zero-point fluctuations) [12]. While optomechanical systems have assumed a wide range of physical systems, including toroidal resonators, nanobeams, membranes and others, the basic principle involves coupling the amplitude of a mechanical oscillator to the resonant frequency of an optical cavity mode [4].

Crystals of laser-cooled, trapped ions behave as atomic-scale mechanical oscillators [13–15] with tunable oscillator modes and high quality factors ($> 10^4$). Furthermore, laser cooling enables ground state cooling of these oscillators. Trapped-ion crystals therefore provide an ideal experimental platform for investigating the fundamental limits of amplitude sensing, but to date there have only been a handful of investigations [14–17]. References [14–16] demonstrate the detection of amplitudes larger than the zero-point fluctuations of the trapped ion oscillator, while [17] reports on injection locking of optically excited mechanical oscillations of a single trapped ion seeded by a weak drive.

In this Letter we experimentally and theoretically analyze a technique to measure the center-of-mass (COM) motion of a two-dimensional, trapped-ion crystal of ∼100 ions with a sensitivity several orders of magnitude below z_{ZPT}. Instead of coupling the motion to an optical cavity mode, we employ a time-varying spin-dependent force $F_0 \cos(\mu t)$ that couples the amplitude of the COM motion with the internal spin degree of freedom of the ions [18, 19]. When the frequency μ matches the frequency ω of an imposed COM oscillation, $Z_c \cos(\omega t)$, spin precession proportional to Z_c occurs, which we read out at the end of the measurement with a precision imposed by spin projection noise [20]. Analogous to optomechanical coupling, here the amplitude of the trapped-ion oscillator produces, in the presence of the spin-dependent force, a shift in the frequency of the spin degree of freedom of the trapped ions.

As we show below, our technique provides a strong, discrete measurement of a single quadrature of the COM motion sensed during the application of the spin-dependent force. To determine the read-out imprecision in a regime free from thermal noise, we perform measurements where ω is far from resonance with the trap axial frequency ω_z. Finally, we implement a protocol where the phase of the measured quadrature randomly varies from one realization of the experiment to the next, appropriate for sensing an unknown force whose phase was unknown or not stable. We detect amplitudes Z_c of 500 pm in a single measurement - an imprecision below z_{ZPT} - and as small as 50 pm with 16 s of integration. Here $z_{ZPT} \equiv \frac{1}{\sqrt{N}}\sqrt{\frac{\hbar}{2m\omega_z}} \approx 2\,\mathrm{nm}$ for $N = 100$ and the parameters of our set-up. From the good theoretical understanding of these limits, we estimate a 75 pm ($\sim 0.04 \times z_{ZPT}$) single-measurement readout imprecision and a sensitivity of ~ 20 pm/$\sqrt{\mathrm{Hz}}$ for a phase-coherent protocol that repeatedly measures the same quadrature of motion. The use of spin-squeezed states, recently demonstrated in this

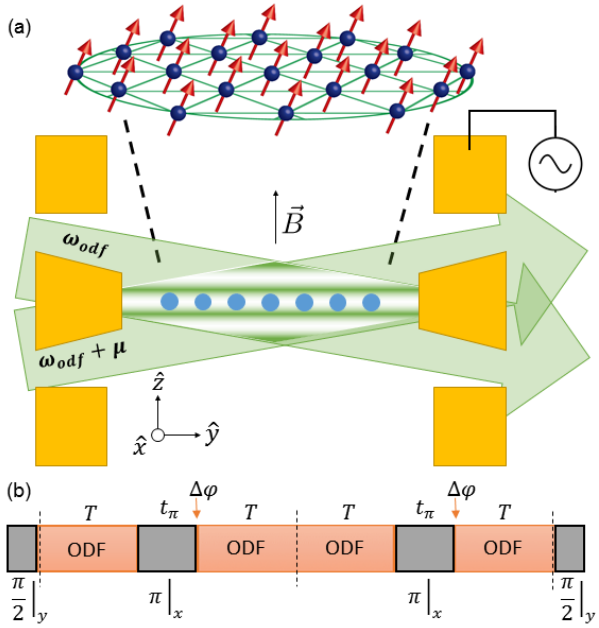

FIG. 1. (a) Representation of ion spins arranged in a 2D triangular lattice, along with a cross-sectional illustration of the Penning trap, characterized by an axial magnetic field $B = 4.45$ T and an axial trap frequency $\omega_z = 2\pi \times 1.57$ MHz. The blue dots represent ions. Cylindrical electrodes (yellow) generate a harmonic confining potential along the $\hat{z}$-axis. Radial confinement is provided by the Lorentz force from $\vec{E} \times \vec{B}$-induced rotation in the axial magnetic field. The beams generating the spin-dependent optical dipole force (green arrows) cross the ion plane at $\pm 10^\circ$, forming a 1D, traveling-wave optical lattice (green lines) with a 0.9 μm wavelength. Doppler cooling beams (not shown) are directed along $\hat{y}$ and $\hat{z}$. An AC voltage source is connected to the trap endcap and used to drive a calibrated axial oscillation. (b) CPMG sequence used to detect spin precession produced by COM motion resonant with the ODF. Orange blocks represent ODF pulses and grey microwave rotations. Doppler cooling and spin state detection occur before and after this sequence, respectively. After each π-pulse, the ODF phase is advanced by $\Delta\varphi = \mu(T + t_\pi)$ in a modulation scheme discussed in [22]. For $\mu/2\pi = (2n+1)/(2(T + t_\pi))$, $\Delta\varphi = \pi$, and therefore spin precession is coherently accumulated for $\omega/2\pi = (2n+1)/(2(T + t_\pi))$. Dashed lines indicate the m segments of the sequence, here $m = 2$. We make use of an $m = 8$ CPMG sequence for Figs. (2)-(4).

system [21], can provide an additional enhancement by reducing projection noise of the readout .

Our experimental apparatus, described in Fig. 1 and [18, 21], consists of $N \sim 100$ $^9\mathrm{Be}^+$ ions laser-cooled to the Doppler limit of 0.5 mK and confined to a single-plane Coulomb crystal in a Penning trap. The spin-1/2 degree of freedom is the $^2S_{1/2}$ ground-state valence electron spin $|\uparrow\rangle$ ($|\downarrow\rangle$) $\equiv |m_s = +1/2\rangle$ ($|m_s = -1/2\rangle$). In the magnetic field of the Penning trap, the ground state is split by 124 GHz. A resonant microwave source is used to perform global rotations of the spin ensemble. A pair of laser beams, detuned from the nearest optical transitions by $\sim$20 GHz, interfere to form a one-dimensional (1D) optical lattice. The resulting spin-dependent optical dipole force (ODF) couples the spins to the ions' axial motion. Optical pumping prepares the initial state $|\uparrow\rangle_N \equiv |\uparrow\uparrow\cdots\uparrow\rangle$ with high fidelity. At the end of the experiments described here we measure the probability $P_\uparrow$ for an ion spin to be in $|\uparrow\rangle$ from a global measurement of state-dependent resonance fluorescence on the Doppler cooling transition, where spin $|\uparrow\rangle$ ($|\downarrow\rangle$) is bright (dark).

The ODF couples the spin and motional degrees of freedom through the interaction [21]

$$\hat{H}_{ODF} = F_0 \cos(\mu t) \sum_i \hat{z}_i \hat{\sigma}_i^z, \tag{1}$$

where $F_0 = U\,\delta k\, \exp(-\delta k^2 \langle \hat{z}_i^2 \rangle /2)$ is the magnitude of the spin-dependent ODF, μ is the frequency difference between the ODF beams, and $\hat{z}_i$ and $\hat{\sigma}_i^z$ are the position operator and Pauli spin matrix for ion i. Here U (δk) is the zero-to-peak potential (wave vector) of the 1D lattice. The term $\exp(-\delta k^2 \langle \hat{z}_i^2 \rangle /2)$ is the Debye-Waller factor, a reduction in interaction strength due to the departure from the Lamb-Dicke confinement regime [23]. We estimate $\exp(-\delta k^2 \langle \hat{z}_i^2 \rangle /2) \approx 0.86$ for the 0.5 mK Doppler laser cooling limit. The potential U, and therefore F_0, is determined from AC Stark shift measurements on the ions [24].

With a weak RF drive on a trap electrode (see Fig. 1(a)) at a frequency ω far from w_z, we impose a weak, classically driven COM motion of constant amplitude and phase, $\hat{z}_i \rightarrow \hat{z}_i + Z_c \cos(\omega t + \delta)$. With $\delta k Z_c \ll 1$ and assuming $\mu \sim \omega$, we use Eq. (1) to describe the shift in the qubit transition frequency due to the coherent amplitude Z_c,

$$\hat{H}_{ODF} = F_0\, Z_c \cos((\omega - \mu)t + \delta) \sum_i \frac{\hat{\sigma}_i^z}{2}. \tag{2}$$

For $\mu = \omega$ there is a static shift $\Delta(Z_c)$ in the frequency of the qubit transition,

$$\Delta(Z_c) = (F_0/\hbar)\, Z_c \cos(\delta). \tag{3}$$

We measure $\Delta(Z_c)$ from the resulting spin precession in an experiment like that shown in Fig. 1(b). The ions are prepared in $|\uparrow\rangle_N$ followed by a microwave $\pi/2$ pulse about $\hat{y}$ that rotates the spins to the $\hat{x}$ axis. The ODF beams are applied through a Carr-Purcell-Meiboom-Gill (CPMG) sequence with phase jumps, coincident with the microwave π pulses, appropriate for adding the accumulated spin precession [22, 25]. If τ is the total ODF interaction time of the sequence, the resulting spin precession on resonance ($\mu = \omega$) is $\theta = \theta_{max} \cos(\delta)$ where $\theta_{max} \equiv (F_0/\hbar)\, Z_c\, \tau$. After a second $\pi/2$ pulse about $\hat{y}$, the final state readout measures the population of the spins in $|\uparrow\rangle$, $P_\uparrow = \frac{1}{2}[1 - e^{-\Gamma\tau} \cos(\theta)]$. Here Γ is the decay rate from spontaneous emission from the off-resonant

ODF laser beams [26]. We implement a protocol where we ensure that the phase δ randomly varies from one realization of the experiment to the next. Different experimental trials therefore result in a different precession $\theta = \theta_{max}\cos(\delta)$, as indicated in Fig. 3. We measure the decrease (or decoherence) in the average length of the Bloch vector resulting from this random precession, $\langle P_\uparrow \rangle = \frac{1}{2}[1 - e^{-\Gamma\tau}\langle\cos(\theta)\rangle]$. The brackets $\langle\cdot\rangle$ denotes an average over many measurements, and necessitates an average over the random phase δ with the result [27]

$$\langle P_\uparrow \rangle = \frac{1}{2}\left[1 - e^{-\Gamma\tau} J_0(\theta_{max})\right]. \qquad (4)$$

Here J_0 is the zeroth order Bessel function of the first kind. Without the driven COM axial motion, the background depends only on Γ, $\langle P_\uparrow \rangle_{bck} = \frac{1}{2}\left[1 - e^{-\Gamma\tau}\right]$.

To create the steady-state COM axial oscillation $Z_c\cos(\omega t + \delta)$, we applied a continuous AC voltage to an endcap of the Penning trap at a frequency $\omega/(2\pi)$ near 400 kHz. This frequency was chosen because it was far from any mode frequencies of the array, and there were no observed sources of noise. Specifically, application of the ODF interaction with $\mu/(2\pi) \approx 400$ kHz and no RF drive resulted in a background given by $\langle P_\uparrow \rangle_{bck}$. We calibrated the displacement of the ions due to a static voltage applied to the endcap by measuring the resulting movement of the ion crystal in the side-view imaging system. From this calibration, we determine that a 1 V offset results in a 0.97(5) μm displacement of the ions. We estimate that the corrections for using this DC calibration to estimate Z_c for an $\omega/(2\pi) \approx 400$ kHz drive is less than 10%.

To detect small amplitudes with the available F_0 in our set-up, we use up to $m = 8$ ODF-π-ODF segments to extend the spin-precession time out to $\tau \geq 20$ms ($T \geq 1.25$ ms in Fig. 1(b)) while maintaining a background fully characterized by decoherence due to spontaneous emission. Figure 2 shows the emergence of the measured spin precession signal out of the background as the amplitude Z_c is increased from 500 pm to 5 nm. The measured lineshape as a function of $\mu - \omega$ agrees well with the predicted lineshape, detailed in [22], involving no free parameters.

Figure 3 shows the background and the measured resonant ($\mu = \omega$) response to a fixed $Z_c = 485$ pm oscillation as the power in the ODF beam is increased. Agreement with Eq. (4) involving no free parameters is excellent. For both Figs. 2 and 3 the background is accounted for within 6% by independent measurements and determinations of the spontaneous emission decay rates of each ODF beam [24]. At each ODF beam strength F_0/F_{0M}, where F_{0M} is the maximum F_0 possible with our current set-up (~ 40 yN), the amplitude $Z_c = \theta_{max}/(F_0\tau/\hbar)$ can be determined from the difference $\langle P_\uparrow \rangle - \langle P_\uparrow \rangle_{bck}$. We note that $\langle P_\uparrow \rangle - \langle P_\uparrow \rangle_{bck}$ depends on θ^2_{max}. Therefore the sensing protocol described here directly measures Z_c^2. The inset of Fig. 3 shows a determination of Z_c^2 for a range

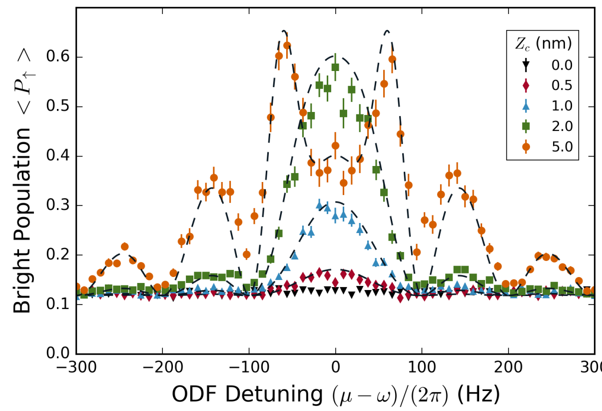

FIG. 2. Lineshape of the spin precession signal for amplitudes Z_c of 500 pm (red diamonds), 1 nm (blue triangles), 2 nm (green squares), and 5 nm (orange circles) for $\tau = 20$ ms. Black triangles are the background, with the drive turned off. Dashed lines are theoretical predictions with no free parameters. Error bars represent standard error. Here $N = 90$ and $F_0/F_{0M} = 0.2$

of ODF strengths F_0/F_{0M}. The uncertainties were determined from the measured noise of the $\langle P_\uparrow \rangle - \langle P_\uparrow \rangle_{bck}$ measurements using standard error propagation [22]. These uncertainties go through a minimum, indicating an optimum F_0/F_{0M} value for the determination of Z_c^2.

To explore the ultimate amplitude sensing limits of our protocol, we performed repeated pairs of $P_\uparrow$ measurements, first with $Z_c = 0$ (i.e. no off-resonant drive on the trap endcap) to get the background, and then with $Z_c \neq 0$. For a given Z_c, 3,000 pairs of measurements were used to determine the average difference $\langle P_\uparrow \rangle - \langle P_\uparrow \rangle_{bck}$ and the standard deviation $\delta\left(P_\uparrow - P_{\uparrow,bck}\right)$ of the difference for a single pair of measurements. For each Z_c, F_0/F_{0M} was set close to the value that maximizes the signal-to-noise ratio of the Z_c^2 determination. This occurs for relatively small θ_{max} such that $\frac{1}{2}\left(1 - J_0\left(\theta_{max}\right)\right) \approx \theta^2_{max}/8$, leading to the expression

$$\frac{Z_c^2}{\delta Z_c^2} \approx \frac{\langle P_\uparrow \rangle - \langle P_\uparrow \rangle_{bck}}{\delta\left(P_\uparrow - P_{\uparrow,bck}\right)}. \qquad (5)$$

for the signal-to-noise ratio of a determination of Z_c^2 from a single pair of $P_\uparrow$, $P_{\uparrow,bck}$ measurements. Figure 4 displays Eq. (5) from measurements made with Z_c ranging from 10 nm to as small as 0.025 nm. Excellent agreement is obtained with a model (dashed red line) that assumes the only sources of noise are projection noise in the spin state detection and fluctuations in $P_\uparrow$ produced by random variation in the phase δ between the COM motion and the ODF from one shot to the next.

For amplitudes $Z_c \gtrsim 500$ pm, noise due to different realizations of the phase δ dominates. This situation is depicted by the middle Bloch sphere of Fig. 3. The fluctuations in $P_\uparrow$ due to different realizations of δ are

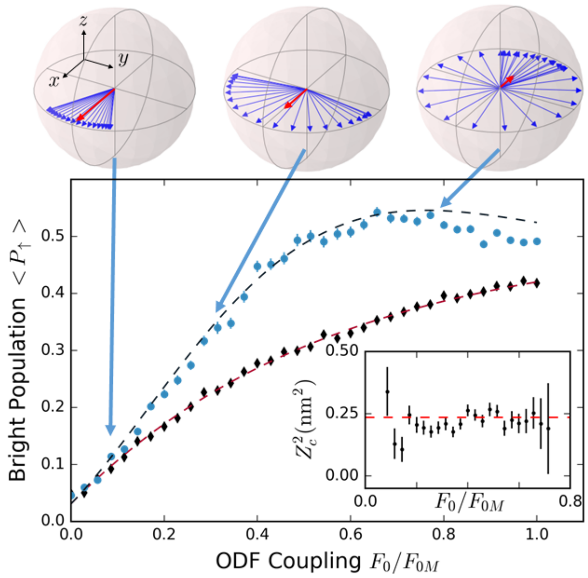

FIG. 3. **Top:** Bloch sphere representation of spin dephasing for $Z_c = 485$ pm. Each blue vector represents an experimental trial with a different phase δ (see text). From left to right, the spread in the blue vectors corresponds to $\theta_{max} = 0.470, 1.41, 3.62$ and $F_0/F_{0M} = 0.1, 0.3, 0.77$, where F_{0M} is the maximum optical-dipole force. Our experiment measures the length of the Bloch vector averaged over many trials, denoted by the thick red vector. **Main plot:** As a function of measurement strength (ODF power), the background (black diamonds) with no applied drive and signal (blue points) for a 485 pm amplitude and total ODF interaction time $\tau = 24$ ms is shown. The red dashed line is a fit to the background. The black dashed line is the theoretical prediction with no free parameters, given the background fit. Here $N = 75$ and $F_{0M} = 41.3$ yN. **Inset:** Black points are experimentally determined values for Z_c^2. Red dashed line is the calibrated value of Z_c^2. Error bars represent standard error.

comparable to signal $\langle P_\uparrow \rangle - \langle P_\uparrow \rangle_{bck}$, limiting the signal-to-noise of a single measurement of Z_c^2 to ~ 1. As Z_c decreases, this noise and the signal decrease, while projection noise stays approximately the same, resulting in a decreasing $Z_c^2/\delta Z_c^2$. We analyze this limiting sensitivity for our protocol in [22] and show that it depends on the ratio $\xi \equiv \Gamma/(U/\hbar)$ of the spontaneous decay to the 1D lattice potential. For our set-up, $\xi = 1.156 \times 10^{-3}$, resulting in a limiting sensitivity of

$$\left.\frac{Z_c^2}{\delta Z_c^2}\right|_{\text{limiting}} = \left[\frac{Z_c}{0.2\ \text{nm}}\right]^2 \tag{6}$$

for $N = 85$ ions of Fig. 4. Equation (6), displayed as the blue line in Fig. 4, agrees well with the measurements and the more complete calculation of $Z_c^2/\delta Z_c^2$. The slope of 2 is a result of being limited by a constant readout noise of the spins (here projection noise), while the intercept is set by ξ, δk, and N [22]. We perform approximately 16 measurements in 1 s, so the single measurement $Z_c^2/\delta Z_c^2$

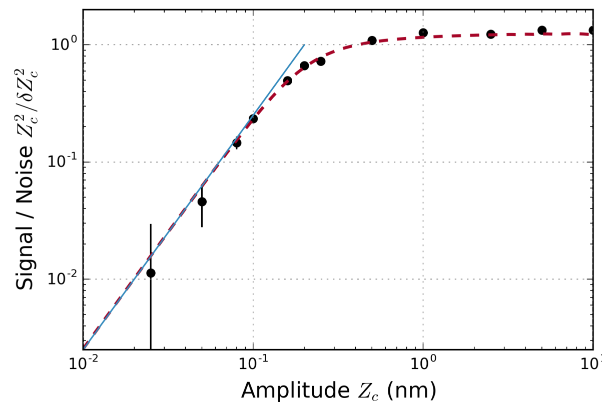

FIG. 4. Amplitude sensing limits. Black points are experimentally determined values of signal-to-noise for single measurements of Z_c^2 as a function of the displacement amplitude. Our measurement for $Z_c = 25$ pm is consistent with zero. Red dashed line is the theoretical prediction for the signal-to-noise including projection noise and relative phase fluctuations. Blue solid line is the limiting signal-to-noise for small amplitudes assuming only projection noise and $\xi = 1.156 \times 10^{-3}$. Error bars represent standard error. Here N = 85.

of Eq. (6) corresponds to a long averaging time sensitivity of $(100\ \text{pm})^2/\sqrt{\text{Hz}}$ (recall that our protocol measures Z_c^2).

Figure 4 documents a good understanding of the sensing limits of our protocol in terms of projection noise in the spin state detection and the ratio ξ of the spontaneous decay rate to the ODF potential. Equation (6) scales as $1/\xi^2$, resulting in significant improvements for set-ups with less spontaneous decay. Phase-coherent amplitude sensing that repeatedly measures the same quadrature of motion can be realized with spin-dependent optical dipole forces and trapped ions [28, 29], and provides a substantial improvement in sensitivity. With the same level of spontaneous emission as our set-up ($\xi = 1.156 \times 10^{-3}$), we estimate a single measurement imprecision of 74 pm for $N = 100$, almost 30 times smaller than the zero-point fluctuations, resulting in a long averaging time sensitivity of $\sim 18\ \text{pm}/\sqrt{\text{Hz}}$.

The 50 pm amplitude detected in Fig. 4 at a frequency ω far from resonance corresponds to an electric field detection of 0.46 mV/m or 73 yN/ion. These force and electric field sensitivities can be improved by the Q of the COM mode by probing near resonance with ω_z. Quality factors $Q \sim 10^6$ should be possible with trapped ion COM modes. The detection of a 20 pm amplitude resulting from a 100 ms coherent drive on the 1.57 MHz COM mode is sensitive to a force/ion of 5×10^{-5} yN corresponding to an electric field of 0.35 nV/m. This requires the use of a protocol to evade back action when probing on resonance [30]. Electric field sensing below ~ 0.1 nV/m provides an opportunity to search for hidden photon dark matter [31, 32], although shielding effects must be carefully considered. Ion traps typically operate with frequencies ω_z in the 50 kHz to 5 MHz range, providing a sensitivity to hidden photon masses in the 2×10^{-10} eV to 2×10^{-8} eV range.

In summary, we have presented a technique for amplitude sensing below the zero-point fluctuations with a trapped ion mechanical oscillator. By coupling the spin and motional degrees of freedom of the ions, a single quadrature of the motional state of the ions may be sensitively read out. We implement a protocol where the phase of the measured quadrature randomly varies, detecting a 500 pm amplitude in a single measurement and demonstrating a long measurement time sensitivity of $(100\,\mathrm{pm})^2/\sqrt{\mathrm{Hz}}$. Modifications of our set-up should enable the implementation of a phase-coherent protocol and a single measurement imprecision of 74 pm for N=100 ions, providing opportunities for trapped ion mechanical oscillators to explore the quantum limits of amplitude and force sensing.

We thank V. Sudhir, R. Ozeri, S. Kotler, and J. Teufel for stimulating discussions. K.G. is supported by NSF grant PHY 1521080.

* kevin.gilmore@colorado.edu
† john.bollinger@nist.gov

[1] J. Weber, Physical Review Letters **17**, 1228 (1966).
[2] C. M. Caves, Physical Review Letters **45**, 75 (1980).
[3] B. P. Abbott *et al.*, Phys. Rev. Lett. **116**, 061102 (2016).
[4] M. Aspelmeyer, T. J. Kippenberg, and F. Marquardt, Reviews of Modern Physics **86**, 1391 (2014).
[5] H.-J. Butt, B. Cappella, and M. Kappl, Surface Science Reports **59**, 1 (2005).
[6] T. A. Palomaki, J. W. Harlow, J. D. Teufel, R. W. Simmonds, and K. W. Lehnert, Nature **495**, 210 (2013).
[7] J. D. Teufel, T. Donner, M. A. Castellanos-Beltran, J. W. Harlow, and K. W. Lehnert, Nature Nanotechnology **4**, 820 (2009).
[8] G. Anetsberger, O. Arcizet, Q. P. Unterreithmeier, R. Rivière, A. Schliesser, E. M. Weig, J. P. Kotthaus, and T. J. Kippenberg, Nature Physics **5**, 909 (2009).
[9] T. Westphal, D. Friedrich, H. Kaufer, K. Yamamoto, S. Goßler, H. Müller-Ebhardt, S. L. Danilishin, F. Y. Khalili, K. Danzmann, and R. Schnabel, Physical Review A **85**, 063806 (2012).
[10] S. Schreppler, N. Spethmann, N. Brahms, T. Botter, M. Barrios, and D. M. Stamper-Kurn, Science **344**, 1486 (2014).
[11] N. S. Kampel, R. W. Peterson, R. Fischer, P. L. Yu, K. Cicak, R. W. Simmonds, K. W. Lehnert, and C. A. Regal, (2016), arXiv:1607.06831.
[12] D. J. Wilson, V. Sudhir, N. Piro, R. Schilling, a. Ghadimi, and T. J. Kippenberg, Nature **524**, 325 (2014).
[13] J. D. Jost, J. P. Home, J. M. Amini, D. Hanneke, R. Ozeri, C. Langer, J. J. Bollinger, D. Leibfried, and D. J. Wineland, Nature **459**, 683 (2009).
[14] M. J. Biercuk, H. Uys, J. W. Britton, A. P. VanDevender, and J. J. Bollinger, Nature Nanotechnology **5**, 646 (2010).
[15] B. C. Sawyer, J. W. Britton, A. C. Keith, C.-C. J. Wang, J. K. Freericks, H. Uys, M. J. Biercuk, and J. J. Bollinger, Physical Review Letters **108**, 213003 (2012).
[16] R. Shaniv and R. Ozeri, Nature Communications **8**, 14157 (2017).
[17] S. Knünz, M. Herrmann, V. Batteiger, G. Saathoff, T. W. Hänsch, K. Vahala, and T. Udem, Physical Review Letters **105**, 013004 (2010).
[18] B. C. Sawyer, J. W. Britton, and J. J. Bollinger, Physical Review A **89**, 033408 (2014).
[19] P. A. Ivanov, Physical Review A **94**, 022330 (2016).
[20] W. M. Itano, J. C. Bergquist, J. J. Bollinger, J. M. Gilligan, D. J. Heinzen, F. L. Moore, M. G. Raizen, and D. J. Wineland, Physical Review A **47**, 3554 (1993).
[21] J. G. Bohnet, B. C. Sawyer, J. W. Britton, M. L. Wall, A. M. Rey, M. Foss-Feig, and J. J. Bollinger, Science **352**, 1297 (2016).
[22] See Supplemental Material for technical details and derivations.
[23] D. J. Wineland, C. Monroe, W. M. Itano, D. Leibfried, B. E. King, and D. M. Meekhof, Journal of Research of the National Institute of Standards and Technology **103**, 259 (1998).
[24] J. W. Britton, B. C. Sawyer, A. C. Keith, C.-C. J. Wang, J. K. Freericks, H. Uys, M. J. Biercuk, and J. J. Bollinger, Nature **484**, 489 (2012).
[25] S. Kotler, N. Akerman, Y. Glickman, A. Keselman, and R. Ozeri, Nature **473**, 61 (2011).
[26] H. Uys, M. J. Biercuk, a. P. Vandevender, C. Ospelkaus, D. Meiser, R. Ozeri, and J. J. Bollinger, Physical Review Letters **105**, 200401 (2010).
[27] S. Kotler, N. Akerman, Y. Glickman, and R. Ozeri, Physical Review Letters **110**, 110503 (2013).
[28] D. B. Hume, C. W. Chou, D. R. Leibrandt, M. J. Thorpe, D. J. Wineland, and T. Rosenband, Physical Review Letters **107**, 243902 (2011).
[29] M. J. Biercuk, H. Uys, J. W. Britton, a. P. Vandevender, and J. J. Bollinger, Optics express **19**, 10304 (2011).
[30] C. Hempel, B. P. Lanyon, P. Jurcevic, R. Gerritsma, R. Blatt, and C. F. Roos, Nature Photonics **7**, 630 (2013).
[31] P. Arias, D. Cadamuro, M. Goodsell, J. Jaeckel, J. Redondo, and A. Ringwald, Journal of Cosmology and Astroparticle Physics **2012**, 013 (2012).
[32] S. Chaudhuri, P. W. Graham, K. Irwin, J. Mardon, S. Rajendran, and Y. Zhao, Physical Review D **92**, 075012 (2015).

INTRODUCTION

In this supplemental material we provide detailed derivations for a number of theoretical formulas and results of the main text. Specifically, in the first section we derive Eq. (2) for the optical dipole force (ODF) Hamiltonian of our system and explain in more detail our modulation scheme. In the second section we derive the lineshape function used in Fig. 2 of the main text. In section 3 we describe the formalism used to determine the optimum signal-to-noise ratio for a measurement of Z_c^2 used to generate the theoretical curve in Fig. 4 of the main text. We also derive the sensitivity limits for phase-incoherent amplitude sensing, where the phase difference between the driven motion and the ODF randomly varies from one realization of the experiment to the next. We show how these limits depend on $\Gamma/(U/\hbar)$, δk, and N. Finally, in section 4 we consider the amplitude sensing limits assuming phase coherence between the spin-dependent force and the driven amplitude.

CONTENTS

1. ODF HAMILTONIAN WITH CLASSICALLY DRIVEN MOTION

Figure 1 shows the Carr-Purcell-Meiboom-Gill (CPMG) sequence used to apply the 1D optical lattice. The interaction of the spin degree of freedom with the 1D optical lattice is given by

$$\hat{H}_{ODF} = U\sum_i \sin(\delta k\cdot\hat{z}_i - \mu t + \phi)\hat{\sigma}_i^z = U\sum_i \sin(\delta k\cdot\hat{z}_i)\cos(\mu t-\phi)\hat{\sigma}_i^z - U\sum_i \cos(\delta k\cdot\hat{z}_i)\sin(\mu t-\phi)\hat{\sigma}_i^z. \quad (1)$$

Here we explicitly include a phase ϕ for the lattice potential. Without loss of generality, we assumed $\phi = 0$ in the main text. If $\delta k\,\langle\hat{z}_i\rangle \ll 1$, then $\langle\cos(\delta k\cdot\hat{z}_i)\rangle \sim 1$, and the spin precession due to the second term will be bounded by $(U/\hbar)/\mu$.

Typically, $(U/\hbar)/\mu \ll 1$ and thus this term is ignored in most treatments. At low frequencies $\mu \le U/\hbar$ this term could be important, but it may be canceled by advancing the phase of the ODF by $\Delta\phi = \mu(T+t_\pi)$ at each microwave $\pi-$pulse of the CPMG sequence (see Fig. 1). When $\mu/2\pi = (2n+1)/(2(T+t_\pi))$, $\Delta\varphi = \pi$ and we recover the quantum lock-in phase advance of [1]. This phase advance coherently accumulates spin precession from the first term of Eq. (1) when $\omega/2\pi = (2n+1)/(2(T+t_\pi))$. The term that survives our modulation scheme is

$$\hat{H}_{ODF} \simeq U\sum_i \sin(\delta k\cdot\hat{z}_i)\cos(\mu t-\phi)\hat{\sigma}_i^z. \quad (2)$$

We now impose a weak, classically driven COM motion of constant amplitude and phase $\hat{z}_i \to \hat{z}_i + Z_c\cos(\omega t+\delta)$. This can be thought of as the center of the Penning trap being moved by $\pm Z_c$ at a frequency ω far from the trap axial frequency ω_z. With $\delta k\, Z_c \ll 1$, we obtain

$$\hat{H}_{ODF} \simeq U\sum_i \left(\delta k\, Z_c\cos(\delta k\cdot\hat{z}_i)\cos(\omega t+\delta)\cos(\mu t-\phi) + \sin(\delta k\cdot\hat{z}_i)\cos(\mu t-\phi)\right)\hat{\sigma}_i^z. \quad (3)$$

The second term of Eq. (3) is the usual term that gives rise to spin-motion entanglement with the drumhead modes and to effective spin-spin interactions [2, 3]. We assume we can neglect this term because we tune μ far from any drumhead modes.

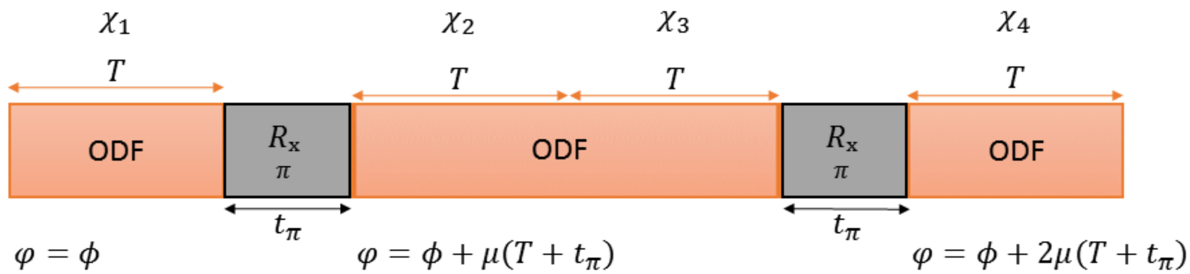

FIG. 1. $m = 2$ CPMG sequence with total ODF interaction time $4T$. φ is the phase of the ODF beatnote. The term labels represent the periods over which the accumulated phase is considered in the text.

The $\cos(\delta k \cdot \hat{z}_i)$ factor in the first term of Eq. (3) equals one deep in the Lamb-Dicke confimenent regime. Here we account for the possibility of not being deep in the Lamb-Dicke confinement regime. In this case, and assuming a thermal distribution of modes, $\langle \cos(\delta k \cdot \hat{z}_i) \rangle = \exp(-\delta k^2 \left\langle \hat{z}_i^2 \right\rangle /2)$. This factor is known as the Debye-Waller factor (DWF). For our conditions all ions have approximately the same Debye-Waller factor, DWF ≈ 0.86 [3].

With $\mu \sim \omega$, Eq. (3) can be written as

$$\hat{H}_{ODF} = (U \cdot \delta k \cdot \mathrm{DWF})\, Z_c \cos((\omega - \mu)t + \delta - \phi) \sum_i \frac{\hat{\sigma}_i^z}{2}, \tag{4}$$

which is Eq. (2) of the main text with $F_0 = U \cdot \delta k \cdot \mathrm{DWF}$.

2. LINESHAPE

To model the lineshape of the signal, it is necessary to account for the accumulated phase due to the spin-dependent ODF potential without making the simplification that $\omega = \mu$. This results in a characteristic response function for each sequence. For this Letter, we used an $m = 8$ CPMG sequence, as shown in Fig. 1 in the main text and also Fig. 1 of this supplemental material. In the following, we derive the lineshape of this sequence, seen in Fig. 2 of the main text. In general, for an $m - \pi$ pulse CPMG sequence it is necessary to calculate the phase evolution during $2m$ terms of length T, for a total interaction time of $2m$T. For simplicity, we first derive the lineshape for the $m = 2$ CPMG sequence (Fig. 1).

For a delta function source $Z_c \cos(\omega t + \delta)$,

$$\theta(\mu) = F_0\, Z_c \frac{2 \sin\left(\frac{1}{2}\,(\omega - \mu)\, T\right)}{(\omega - \mu)} f(\mu, \omega) \tag{5}$$

where $f(\mu, \omega)$ is determined by the phase accumulated through a particular sequence. In the case of the $m = 2$ CPMG sequence, the phase accumulated through 4 terms corresponding to 4 separate applications of the ODF (Fig. 1) must be considered:

$$\chi_1 = \cos\left[(\omega - \mu)\, \frac{T}{2} + \delta + \phi\right], \tag{6}$$

$$\chi_2 = -\cos\left[(\omega - \mu)\left(\frac{3T}{2} + t_\pi\right) + \delta + \phi + \mu(T + t_\pi)\right], \tag{7}$$

$$\chi_3 = -\cos\left[(\omega - \mu)\left(\frac{5T}{2} + t_\pi\right) + \delta + \phi + \mu(T + t_\pi)\right], \tag{8}$$

$$\chi_4 = \cos\left[(\omega-\mu)\left(\frac{7T}{2}+2t_\pi\right)+\delta+\phi+2\mu(T+t_\pi)\right]. \tag{9}$$

Note these terms now include a phase ϕ for the ODF interaction, which in the main text we set to zero with no loss of generality. Adding these terms up, pairwise:

$$\chi_1+\chi_2 = 2\sin\left(\frac{1}{2}\left[(\omega-\mu)\left(T+t_\pi\right)+\mu(T+t_\pi)\right]\right)\sin\left[(\omega-\mu)\left(T+\frac{t_\pi}{2}\right)+\delta+\phi+\frac{\mu(T+t_\pi)}{2}\right], \tag{10}$$

$$\chi_3+\chi_4 = -2\sin\left(\frac{1}{2}\left[(\omega-\mu)\left(T+t_\pi\right)+\mu(T+t_\pi)\right]\right)\sin\left[(\omega-\mu)\left(3T+\frac{3t_\pi}{2}\right)+\delta+\phi+\frac{3\mu(T+t_\pi)}{2}\right]. \tag{11}$$

$f(\mu,\omega)$ is the sum of all four terms:

$$f(\mu,\omega) = 2\sin\left(\frac{\omega}{2}\left(T+t_\pi\right)\right)\left[\sin\left(\xi+\delta+\phi\right)-\sin\left(3\xi+\delta+\phi\right)\right], \tag{12}$$

where $\xi = (\omega-\mu)(T+\frac{t_\pi}{2})+\frac{\mu(T+t_\pi)}{2} = \frac{1}{2}\left(\omega(T+t_\pi)+T\left(\omega-\mu\right)\right)$. Then, simplifying:

$$f(\mu,\omega) = 2\sin\left(\frac{\omega}{2}\left(T+t_\pi\right)\right)2\sin\left(-\xi\right)\cos\left(2\xi+\delta+\phi\right). \tag{13}$$

Using Eqs. 11 and 3,

$$\theta(\mu) = DWF\cdot U\cdot\delta k\cdot Z_c\cdot T\,\mathrm{sinc}\left(\frac{T}{2}\left(\omega-\mu\right)\right)4\sin\left(\frac{\omega}{2}\left(T+t_\pi\right)\right)\sin\left(\xi\right)\cos\left(2\xi+\delta+\phi\right). \tag{14}$$

Since $4T=\tau$ for the $m=2$ CPMG

$$\theta(\mu) = \theta_{max}\,\mathrm{sinc}\left(\frac{T}{2}\left(\omega-\mu\right)\right)\sin\left(\frac{\omega}{2}\left(T+t_\pi\right)\right)\sin\left(\xi\right)\cos\left(2\xi+\delta+\phi\right) \tag{15}$$

$\theta_{max}(\mu)$, defined as $\theta(\mu)=\theta_{max}(\mu)\cos\left(2\xi+\delta+\phi\right)$, is the μ-dependent generalization of θ_{max}. From Eq. 13, this is

$$\theta_{max}(\mu) = \theta_{max}\,\mathrm{sinc}\left(\frac{T}{2}\left(\omega-\mu\right)\right)\sin\left(\frac{\omega}{2}\left(T+t_\pi\right)\right)\sin\left(\xi\right). \tag{16}$$

For the $m=8$ CPMG sequence the same procedure is used, but now with 16 periods of accumulated phase. We obtain:

$$\theta_{max}(\mu) = \theta_{max}\,\mathrm{sinc}\left(\frac{T}{2}\left(\omega-\mu\right)\right)\sin\left(\frac{\omega}{2}\left(T+t_\pi\right)\right)\sin(\xi)\cos(2\xi)\cos(4\xi). \tag{17}$$

As shown in the main text, the expression for population in spin-up - now with a dependence on the ODF difference frequency μ - is:

$$\langle P_\uparrow\rangle = \frac{1}{2}\left[1-e^{-\Gamma\tau}J_0(\theta_{max}(\mu))\right]. \tag{18}$$

3. PHASE-INCOHERENT SENSING LIMITS

Here we derive Eq. 6 from the main text and provide additional mathematical background for the phase-incoherent experimental protocol, wherein the phase of the measured quadrature varies randomly from one realization of the experiment to the next. Following earlier discussions, the probability of measuring $|\uparrow\rangle$ at the end of the Ramsey sequence is

$$\langle P_\uparrow \rangle = \frac{1}{2}\left[1 - e^{-\Gamma\tau} J_0\left(\theta_{max}\right)\right] , \tag{19}$$

where $\langle\,\rangle$ denotes an average over many experimental trials and therefore over the random phase between the 1D optical lattice and the classically driven COM motion, and

$$\theta_{max} = \left(F_0/\hbar\right) \cdot Z_c \cdot \tau \,. \tag{20}$$

Defining $G\left(\theta^2_{max}\right) \equiv \left(1 - J_0\left(\theta_{max}\right)\right)/2$ and denoting $\langle P_\uparrow\rangle_{bck} = \left[1 - e^{-\Gamma\tau}\right]/2$ as the probability of measuring $|\uparrow\rangle$ at the end of the sequence in the absence of a classically driven motion, θ^2_{max} can be determined from a measurement of the difference $\langle P_\uparrow\rangle - \langle P_\uparrow\rangle_{bck}$ through

$$G\left(\theta^2_{max}\right) = e^{\Gamma\tau}\left(\langle P_\uparrow\rangle - \langle P_\uparrow\rangle_{bck}\right) \,. \tag{21}$$

The standard deviation $\delta\theta^2_{max}$ in estimating θ^2_{max} is determined from the standard deviation $\delta\left(P_\uparrow - P_{\uparrow,bck}\right)$ of the $\langle P_\uparrow\rangle - \langle P_\uparrow\rangle_{bck}$ difference measurements through

$$\delta\theta^2_{max} = \frac{e^{\Gamma\tau}\delta\left(\langle P_\uparrow\rangle - \langle P_\uparrow\rangle_{bck}\right)}{\frac{\mathrm{d}G\left(\theta^2_{max}\right)}{d\theta^2_{max}}} \,. \tag{22}$$

The signal-to-noise ratio of a measurement of θ^2_{max} (and therefore Z^2_c) is then $\theta^2_{max}/\delta\theta^2_{max}$. In general this signal-to-noise ratio depends on θ^2_{max} and the experimental parameters $U\cdot\tau$, $\Gamma\cdot\tau$, δk, and N.

We use Eq. (22) to theoretically estimate $\theta^2_{max}/\delta\theta^2_{max}$ and the amplitude sensing limits. We assume the only sources of noise are projection noise in the measurement of the spin state and fluctuations in $P_\uparrow$ due to the random variation in the relative phase of the 1D optical lattice and the driven COM motion. In this case $\delta\left(P_\uparrow - P_{\uparrow,bck}\right) = \sqrt{\delta\langle P_\uparrow\rangle^2 + \delta\langle P_\uparrow\rangle^2_{bck}}$ where the relevant variances are

$$\delta\langle P_\uparrow\rangle^2_{bck} = \frac{1}{N}\langle P_\uparrow\rangle_{bck}\left(1 - \langle P_\uparrow\rangle_{bck}\right) = \frac{1}{4N}\left(1 - e^{-2\Gamma\tau}\right) \tag{23}$$

and

$$\delta\langle P_\uparrow\rangle^2 = \sigma^2_\phi + \frac{1}{N}\langle P_\uparrow\rangle\left(1 - \langle P_\uparrow\rangle\right) \,. \tag{24}$$

Here N is the number of spins. Equation (23) and the second term in Eq. (24) are projection noise. The variance

$$\sigma^2_\phi = \left\langle P^2_\uparrow - \langle P_\uparrow\rangle^2\right\rangle = \frac{e^{-2\Gamma\tau}}{8}\left(1 + J_0\left(2\theta_{max}\right) - 2J_0\left(\theta_{max}\right)^2\right) \tag{25}$$

is due to the random variation in the relative phase of the 1D optical lattice and the driven COM motion. For our set-up, $DWF = \exp(-\delta k^2\left\langle\hat{z}^2_i\right\rangle/2) = 0.86$ and $\delta k = 2\pi/\left(900\,\mathrm{nm}\right)$ are fixed, the decoherence Γ is a function of U, $\Gamma = \xi\left(U/\hbar\right)$ where $\xi = 1.156\times10^{-3}$, and $F_0 = DWF\cdot U\cdot\delta k$. For a given Z_c we use Eqs. (20) and (22)-(25) to find the optimum $\theta^2_{max}/\delta\theta^2_{max}$ as a function of $\left(U\tau\right)/\hbar$. This optimum value is the theoretical curve plotted in Figure 4 of the main text.

One can show that $\theta^2_{max}/\delta\theta^2_{max}$ is optimized for relatively small values of θ^2_{max} where $G\left(\theta^2_{max}\right) \approx \theta^2_{max}/8$ is a good approximation. This leads to some simplifications for Eqs. (21) and (22),

$$\theta^2_{max} \approx 8e^{\Gamma\tau}\left(\langle P_\uparrow\rangle - \langle P_\uparrow\rangle_{bck}\right) \tag{26}$$

and

$$\delta\theta^2_{max} \approx 8e^{\Gamma\tau}\delta\left(P_\uparrow - P_{\uparrow,bck}\right) , \tag{27}$$

and to the following estimate for the signal-to-noise ratio of a single measurement,

$$\frac{\theta_{max}^2}{\delta\theta_{max}^2} \approx \frac{\langle P_\uparrow\rangle - \langle P_\uparrow\rangle_{bck}}{\delta\left(P_\uparrow - P_{\uparrow,bck}\right)} \, . \tag{28}$$

Figure (4) of the main text uses Eq. (28), along with repeated measurements of $P_\uparrow - P_{\uparrow,bck}$, to experimentally determine the signal-to-noise ratio as a function of the amplitude Z_c of the COM motion.

Finally we use Eqs. (20) and (22)-(25) to calculate the sensing limits for very small Z_c. For small Z_c the variance σ_ϕ^2 can be neglected compared to projection noise and $\delta\langle P_\uparrow\rangle^2 \approx \delta\langle P_\uparrow\rangle_{bck}^2$. In this case we obtain the following expression for the signal-to-noise ratio,

$$\frac{Z_c^2}{\delta Z_c^2} = \frac{\sqrt{N}}{4\sqrt{2}} \frac{DWF^2 \cdot \left(\delta k\, Z_c\right)^2 \left(U\tau/\hbar\right)^2}{\sqrt{e^{2\xi U\tau/\hbar} - 1}} \, . \tag{29}$$

Equation (29) is maximized for $\xi U\tau \approx 1.9603$. With $DWF = 0.86$, $\delta k = 2\pi/\left(900\,\mathrm{nm}\right)$, $\xi = 1.156\times10^{-3}$, and $N = 85$,

$$\left.\frac{\theta_{max}^2}{\delta\theta_{max}^2}\right|_{optimum} = \left[\frac{Z_c}{0.2\,\mathrm{nm}}\right]^2 \, . \tag{30}$$

For our set-up and available ODF power, $\xi U\tau/\hbar \approx 1.9603$ is realized for $\tau \approx 20\,\mathrm{ms}$. A measurement of the signal and a measurement of the background requires $\sim 60\,\mathrm{ms}$, allowing for 16 independent measurements of $P_\uparrow - P_{\uparrow,bck}$ in 1 s. The limiting sensitivity is approximately $\left(100\,\mathrm{pm}\right)^2$ in a 1 s measurement time, or $\left(100\,\mathrm{pm}\right)^2/\sqrt{\mathrm{Hz}}$. We note that the limiting sensitivity is determined by the ratio $\xi = \Gamma/\left(U/\hbar\right)$. In particular, the optimum value for Eq. (29) scales as $1/\xi^2$.

4. PHASE-COHERENT SENSING LIMITS

With appropriate care the phase of the 1D optical lattice can be stable for long periods of time with respect to the ion trapping electrodes [4], enabling repeated phase-coherent sensing of the same quadrature of the COM motion $Z_c\cos(\omega t)$. In this case the same spin precession $\theta_{max} = DWF\cdot(U/\hbar)\cdot\delta k\, Z_c\cdot\tau$ occurs for each experimental trial, which can be detected to first order in θ_{max} (or Z_c) in a CPMG sequence with a $\pi/2$ phase shift between the two $\pi/2$-pulses. Assuming $\sin\left(\theta_{max}\right) \approx \theta_{max}$, appropriate for small amplitudes Z_c, the equivalent phase-coherent sensing expressions for Eqs. (26) and (27) are

$$\theta_{max} = 2e^{\Gamma\tau}\left(\langle P_\uparrow\rangle - \langle P_\uparrow\rangle_{bck}\right) \tag{31}$$

and

$$\delta\theta_{max} = 2e^{\Gamma\tau}\delta\left(P_\uparrow - P_{\uparrow,bck}\right) \, . \tag{32}$$

For a CPMG experiment with a $\pi/2$ phase shift, $\langle P_\uparrow\rangle_{bck} = 1/2$. If projection noise is the only source of noise, then for small Z_c, $\delta\langle P_\uparrow\rangle^2 \approx \delta\langle P_\uparrow\rangle_{bck}^2 = \frac{1}{N}\cdot\frac{1}{2}\cdot\frac{1}{2}$ and $\delta\left(P_\uparrow - P_{\uparrow,bck}\right) \approx \frac{1}{\sqrt{2N}}$. The limiting signal-to-noise ratio $\theta_{max}/\delta\theta_{max}$ of a $\left(P_\uparrow - P_{\uparrow,bck}\right)$ measurement is

$$\frac{\theta_{max}}{\delta\theta_{max}} = DWF\cdot\left(\delta k\, Z_c\right)\cdot\sqrt{\frac{N}{2}}\cdot\frac{(U\tau)}{\hbar}e^{-\xi U\tau/\hbar} \, . \tag{33}$$

Equation (33) is maximized for $\xi U\tau/\hbar = 1$. With $DWF = 0.86$, $\delta k = 2\pi/\left(900\,\mathrm{nm}\right)$, $\xi = 1.156\times10^{-3}$, and $N = 100$,

$$\left.\frac{\theta_{max}}{\delta\theta_{max}}\right|_{optimum} = \frac{Z_c}{0.074\,\mathrm{nm}} \, . \tag{34}$$

With 16 independent measurements of $\langle P_\uparrow\rangle - \langle P_\uparrow\rangle_{bck}$ in 1 s, this corresponds to a limiting sensitivity of $\sim \left(20\,\mathrm{pm}\right)/\sqrt{\mathrm{Hz}}$. The optimum value for the signal-to-ratio of Eq. (33) scales as $1/\xi$. By employing spin-squeezed states that have been demonstrated in this system [3], $\theta_{max}/\delta\theta_{max}$ can be improved by another factor of 2.

Employing this technique to sense motion resonance with the COM mode can lead to the detection of very weak forces and electric fields. The detection of a 20 pm amplitude resulting from a 100 ms coherent drive on the 1.57 MHz COM mode is sensitive to a force/ion of 5×10^{-5} yN corresponding to an electric field of 0.35 nV/m.

* kevin.gilmore@colorado.edu
† john.bollinger@nist.gov
[1] S. Kotler, N. Akerman, Y. Glickman, A. Keselman, and R. Ozeri, Nature **473**, 61 (2011).
[2] J. W. Britton, B. C. Sawyer, A. C. Keith, C.-C. J. Wang, J. K. Freericks, H. Uys, M. J. Biercuk, and J. J. Bollinger, Nature **484**, 489 (2012) (see Supplementary Information).
[3] J. G. Bohnet, B. C. Sawyer, J. W. Britton, M. L. Wall, A. M. Rey, M. Foss-Feig, and J. J. Bollinger, Science **352**, 1297 (2016) (see Supplementary Information).
[4] D. B. Hume, C. W. Chou, D. R. Leibrandt, M. J. Thorpe, D. J. Wineland, and T. Rosenband, Physical Review Letters **107**, 243902 (2011).